Chaotic and regular instantons in helical shell models of turbulence

Massimo De Pietro,[1] Alexei A. Mailybaev,[2] and Luca Biferale[1]

[1]*Dipartimento di Fisica and INFN, Università "Tor Vergata,"*
Via della Ricerca Scientifica 1, 00133 Roma, Italy
[2]*Instituto Nacional de Matemática Pura e Aplicada, Rio de Janeiro, 22460-320 Rio de Janeiro, Brazil*

Shell models of turbulence have a finite-time blowup in the inviscid limit, i.e., the enstrophy diverges while the single-shell velocities stay finite. The signature of this blowup is represented by self-similar instantonic structures traveling coherently through the inertial range. These solutions might influence the energy transfer and the anomalous scaling properties empirically observed for the forced and viscous models. In this paper we present a study of the instantonic solutions for a set of four shell models of turbulence based on the exact decomposition of the Navier-Stokes equations in helical eigenstates. We find that depending on the helical structure of each model, instantons are chaotic or regular. Some instantonic solutions tend to recover mirror symmetry for scales small enough. Models that have anomalous scaling develop regular nonchaotic instantons. Conversely, models that have nonanomalous scaling in the stationary regime are those that have chaotic instantons. The direction of the energy carried by each single instanton tends to coincide with the direction of the energy cascade in the stationary regime. Finally, we find that whenever the small-scale stationary statistics is intermittent, the instanton is less steep than the dimensional Kolmogorov scaling, independently of whether or not it is chaotic. Our findings further support the idea that instantons might be crucial to describe some aspects of the multiscale anomalous statistics of shell models.

I. INTRODUCTION

The phenomenological Kolmogorov theory is able to catch the basic constituents of the energy transfer mechanisms in homogeneous and isotropic turbulence, but it falls short in explaining subtle effects such as intermittency, i.e., the existence of anomalous scaling laws for velocity increments in the limit of high Reynolds numbers [1], where the Reynolds number Re measures the relative importance of inertial and viscous effects. When Re $\to \infty$, a wide separation opens between the scale where forcing and viscous mechanism act, making the problem computationally hard and analytically intractable. Up to now, all attempts to attack the problem for the three-dimensional Navier-Stokes equation (NSE) have failed. As a result, many approximate approaches have been developed in order to gain insights into the transfer mechanisms in turbulent flows. A successful approach is represented by shell models [2–10], especially concerning the existence of intermittency and anomalous scaling laws.

Shell models of turbulence are dynamical models that mimic the NSE in the wave-number space. They are based on a strong reduction of the number of degrees of freedom, dividing and discretizing the Fourier space into a number of shells equally spaced on a logarithmic scale $k_n = k_0 \lambda^n$ (a common choice is $\lambda = 2$ and $k_0 = 1$). Only a few representative variables u_n are kept for each shell of wave numbers. Each variable is meant to represent a typical velocity fluctuation of the original three-dimensional Navier-Stokes field $\delta_r v$ at scale $r \sim 1/k_n$. In this way, a large separation of scales can be achieved with relatively few variables. Furthermore, inspired by the Kolmogorov phenomenology for the direct energy transfer, these models consider only local interactions in Fourier space, connecting dynamical evolution between three generic neighboring modes k_n, k_{n+1}, k_{n+2}. Finally, the models are built in such a way as to have the same inviscid invariants of the original NSE: energy and helicity for models of three-dimensional (3D) turbulence or energy and enstrophy for 2D turbulence.

The success of these models lies in the fact that despite the huge simplifications, they still share many properties with the original Navier-Stokes turbulence, including the development of anomalous scaling laws with values of the scaling exponents very close to the ones measured in 3D turbulence [6–8,11]. Though the turbulence even in such simplified models is far from being understood, shell models remain important in fluid dynamics for accessing detailed properties of energy transfer mechanisms.

In particular, in [12] the issue of intermittency was studied in one popular shell model [7] and it was argued that anomalous scaling exponents of velocity moments can be related to the scaling and statistics of instantons. Instantons are particular solutions of the inviscid equations of motion, intimately connected to the finite-time blowup of the model with an infinite number of shells [13,14]. In the turbulent velocity field they are represented by coherent structures that traverse the inertial range towards large wave numbers. In this work, we attribute the word instanton to a self-similar inviscid structure localized in both time and scale, which is different from the viscous instantonic solutions generated within the Martin-Siggia-Rose formalism and widely studied for the original three-dimensional NSE and for Burgers equations [12–21].

In the following we study the structure of instantonic solutions in four different classes of shell models [22] generalized to have a closer analogy with the original structure of the NSE decomposed on a helical Fourier basis [23]. Helical decomposition of the NSE is useful to disentangle triad interactions that preferentially transfer energy to small or to large scales (forward and backward energy cascades). This statement was recently supported in direct numerical simulation of the NSE with appropriate dynamical mode reduction [24–27] and in the equivalent helical version of shell models [28]. Let us note that instantonic solutions were shown to be closely related to the events preceding a shock formation in compressible flows [29], justifying their relevance also for realistic hydrodynamical systems in the continuum. Such a relation for incompressible flows, as well as for the case of a chaotic instanton, is unknown. Chaotic instantons may turn out to be useful for describing an nonregular behavior in 3D Euler equations, in relation to the open problem of finite-time blowup, and they are also conjectured to describe the Belinsky-Khalatnikov-Lifshitz singularity solution for Einstein's field equations of gravitation [30].

The paper is structured as follows. In Secs. II and III we review the general concepts of helical shell models and define the instantonic solutions for such models. In Secs. IV, V, and VI we show results from numerical simulations, concerning different aspects: the general dynamics of the instantons, their helical structure, and the energy transfers they induce, respectively. Finally, in Sec. VII we discuss our findings and summarize the connections between the instantonic solutions and the stationary dynamics of shell models and real turbulence.

II. HELICAL SHELL MODELS

The three-dimensional incompressible Navier-Stokes equations can be exactly decomposed on a base of positive and negative polarized helical waves [23]. In Fourier space, this helical decomposition for a velocity field reads

$$\mathbf{u}(\mathbf{k}) = u_{\mathbf{k}}^+ \mathbf{h}_{\mathbf{k}}^+ + u_{\mathbf{k}}^- \mathbf{h}_{\mathbf{k}}^-, \tag{1}$$

where for each wave vector $\mathbf{k}$, $\mathbf{h}_{\mathbf{k}}^+$, and $\mathbf{h}_{\mathbf{k}}^-$ are eigenvectors of the curl operator,

$$i\mathbf{k} \times \mathbf{h}_{\mathbf{k}}^s = sk\mathbf{h}_{\mathbf{k}}^s. \tag{2}$$

Such vectors carry, respectively, positive and negative helicity and can be taken as

$$\mathbf{h}_{\mathbf{k}}^s = \boldsymbol{\nu}_{\mathbf{k}} \times \boldsymbol{\kappa} + si\boldsymbol{\nu}_{\mathbf{k}}, \tag{3}$$

where $\mathbf{k} = k\boldsymbol{\kappa}$ and $\boldsymbol{\nu}_{\mathbf{k}}$ is an arbitrary vector orthogonal to $\mathbf{k}$. Then the two fields $u_{\mathbf{k}}^+$ and $u_{\mathbf{k}}^-$ are the projections on the $\mathbf{h}_{\mathbf{k}}^+$ and $\mathbf{h}_{\mathbf{k}}^-$ directions of the Fourier coefficients of the velocity field. Plugging decomposition (1) into the nonlinear term of the NSEs, one can distinguish eight possible nonlinear triadic interactions depending on the signs of the corresponding helical projections [23]. Four out of

TABLE I. Structure and coefficients of the four helical models (4) and (5). The second column lists classes of helical interactions. Without loss of generality, we always choose $a = 1$. These a, b, and c coefficients ensure energy and helicity conservation.

Model	Helical modes coupling	s_1	s_2	s_3	s_4	s_5	s_6	b	c
SM1	$(u_n^+, u_{n+1}^-, u_{n+2}^+)$ or $(u_n^-, u_{n+1}^+, u_{n+2}^-)$	$+$	$-$	$-$	$-$	$-$	$+$	$-1/2$	$1/2$
SM2	$(u_n^+, u_{n+1}^-, u_{n+2}^-)$ or $(u_n^-, u_{n+1}^+, u_{n+2}^+)$	$-$	$-$	$+$	$-$	$+$	$-$	$-5/2$	$-3/2$
SM3	$(u_n^+, u_{n+1}^+, u_{n+2}^-)$ or $(u_n^-, u_{n+1}^-, u_{n+2}^+)$	$-$	$+$	$-$	$+$	$-$	$-$	$-5/6$	$1/6$
SM4	$(u_n^+, u_{n+1}^+, u_{n+2}^+)$ or $(u_n^-, u_{n+1}^-, u_{n+2}^-)$	$+$	$+$	$+$	$+$	$+$	$+$	$-3/2$	$-1/2$

eight interactions are independent, because the interactions with reversed helicities are identical. The four structures of interacting triads will be labeled SM1-4 and they are summarized in the second column of Table I.

It is possible to construct four different shell models with a helicity structure analogous to that of the four subclasses of the original NSEs [22,28]:

$$\dot{u}_n^+ = i\left(ak_{n+1}u_{n+2}^{s_1}u_{n+1}^{s_2*} + bk_n u_{n+1}^{s_3}u_{n-1}^{s_4*} + ck_{n-1}u_{n-1}^{s_5}u_{n-2}^{s_6}\right) + f_n^+ - \nu k_n^2 u_n^+, \tag{4}$$

$$\dot{u}_n^- = i\left(ak_{n+1}u_{n+2}^{-s_1}u_{n+1}^{-s_2*} + bk_n u_{n+1}^{-s_3}u_{n-1}^{-s_4*} + ck_{n-1}u_{n-1}^{-s_5}u_{n-2}^{-s_6}\right) + f_n^- - \nu k_n^2 u_n^-, \tag{5}$$

where $n = 1, 2, \ldots$ are shell indices and u_n^+ and u_n^- are complex shell variables (speeds) corresponding to positive and negative helicity modes. The helical indices $s_i = \pm$ and the coefficients a, b, c can be found in Table I. Note that model SM1 can be split into two identical fully uncoupled models for the variables $u_1^+, u_2^-, u_3^+, \ldots$ and $u_1^-, u_2^+, u_3^-, \ldots$. The same is true for model SM4, where the uncoupled models are $u_1^+, u_2^+, u_3^+, \ldots$ and $u_1^-, u_2^-, u_3^-, \ldots$; models SM2 and SM3, on the contrary, cannot be decoupled. In shell models (4) and (5) both the total energy E and the total helicity H are conserved for zero viscosity and zero forcing (just as in NSEs):

$$E = \sum_{n=1}^{\infty} E_n, \quad H = \sum_{n=1}^{\infty} H_n, \tag{6}$$

where the energy and helicity spectra are

$$E_n = |u_n^+|^2 + |u_n^-|^2, \quad H_n = k_n(|u_n^+|^2 - |u_n^-|^2). \tag{7}$$

Note that any linear combination of models SM1–SM4 conserves the total energy and helicity. The coupling among the four models can be explicitly calculated so as to be consistent with the structure of the NSE [31].

III. FINITE-TIME BLOWUP IN THE INVISCID MODEL

In this paper we are interested in understanding the propagation of fluctuations in the inertial range of scales, i.e., in the inviscid limit. In such a limit, solutions of shell models are characterized by a finite-time infinite growth (blowup) of the enstrophy [13,29,32,33]

$$\Omega(t) \to \infty \quad \text{as } t \to t_c^-. \tag{8}$$

For helical models, the enstrophy is defined as

$$\Omega = \omega^2 = \sum_{n=1}^{\infty} k_n^2(|u_n^+|^2 + |u_n^-|^2), \tag{9}$$

where we also introduced ω as the square root of the enstrophy for further convenience. The dynamical signature of this blowup is a coherent structure that travels from small to large wave numbers in a self-similar manner.

Furthermore, it is possible to find a suitable change of variables that turns the blowup solution into a steady-state traveling wave, which is much easier to study. Concerning the helical models, we introduce the renormalized time τ and shell variables $w_n^{\pm}$, respectively,

$$\frac{d\tau}{dt} = \frac{\omega(t)}{\omega_0}, \quad w_n^{\pm}(\tau) = -\frac{ik_n u_n^{\pm}(t)}{\omega(t)/\omega_0}, \tag{10}$$

where $\Omega_0 = \omega_0^2$ is the initial enstrophy value at $t = \tau = 0$. These variables are designed such that their norm

$$\|w\|^2 = \sum_{n=1}^{\infty}(|w_n^+|^2 + |w_n^-|^2) = \Omega_0 \tag{11}$$

is conserved. With definitions (10) it is possible to rewrite the inviscid and unforced equations (4) and (5) in the form

$$\left(\frac{d}{d\tau} + A(\tau)\right)w_n^+ = a\lambda^{-2}w_{n+2}^{s_1}w_{n+1}^{s_2*} + bw_{n+1}^{s_3}w_{n-1}^{s_4*} - c\lambda^2 w_{n-1}^{s_5}w_{n-2}^{s_6}, \tag{12}$$

$$\left(\frac{d}{d\tau} + A(\tau)\right)w_n^- = a\lambda^{-2}w_{n+2}^{-s_1}w_{n+1}^{-s_2*} + bw_{n+1}^{-s_3}w_{n-1}^{-s_4*} - c\lambda^2 w_{n-1}^{-s_5}w_{n-2}^{-s_6}, \tag{13}$$

where

$$A = \frac{1}{\omega}\frac{d\omega}{d\tau}. \tag{14}$$

For ω (square root of the enstrophy), we get

$$\omega(\tau) = \omega_0 \exp\left(\int_0^{\tau} A(\tau')d\tau'\right). \tag{15}$$

Here we wrote ω as a function of τ, which in turn is a function of original time t. Differentiating (11) with respect to τ and using (12) and (13), one can get an explicit expression for

$$A = \frac{1}{\Omega_0}\sum_n \text{Re}(w_n^{+*}NLT_n^+ + w_n^{-*}NLT_n^-), \tag{16}$$

where NLT_n^+ and NLT_n^- represent the right-hand sides of Eqs. (12) and (13).

This renormalization completely removes the stiffness (exponential decrease in local time scale at increasing shell numbers n) of the original system and maps the blowup limit $t \to t_c^-$ to the infinite limit $\tau \to \infty$, so the solutions are well-defined globally in the renormalized time τ. Note that there is a one-to-one exact correspondence between solutions of the original and renormalized systems, for $t < t_c$.

The blowup can be described asymptotically as an attractor of the renormalized dynamics [34]. For instance, as the norm $\|w\|^2 = \Omega_0$ is conserved, the renormalized system (12) and (13) may have a solitary wave solution

$$w_n^{\pm} = W^{\pm}(n - s\tau), \tag{17}$$

where s represents the wave speed and $W^{\pm}(\xi)$ are functions vanishing as $\xi \to \pm\infty$. Let us introduce the scaling exponent

$$y = \log_{\lambda}\frac{\omega(\tau_1)}{\omega_0} > 0, \quad \tau_1 = 1/s, \tag{18}$$

where the value τ_1 is defined as the renormalized time in which solution (17) travels over a single shell $n \mapsto n + 1$. If $y > 0$, then the traveling wave (17) represents the self-similar finite-time blowup for the original shell variables $u_n^\pm$ given by (10) as [13,34]

$$u_n^\pm = i k_n^{y-1} U^\pm \left[k_n^y (t - t_c) \right],$$
(19)

where

$$U^\pm(t - t_c) = \frac{\omega(\tau)}{\omega_0} W^\pm(-s\tau),$$
(20)

$$t_c = \int_0^\infty \exp \frac{\omega(\tau)}{\omega_0} d\tau' < \infty.$$
(21)

Here the condition $y > 0$ is necessary to ensure the convergence of the integral (21), i.e., the finiteness of the blowup time t_c.

IV. REGULAR AND CHAOTIC INSTANTONS

We have performed a series of numerical integrations of Eqs. (12) and (13), using a standard fourth-order Runge-Kutta scheme. For each model we made a number of simulations with different initial conditions. In the initial conditions, energy was distributed uniformly over a small interval of shell numbers $n = 10, \ldots, 14$; the velocity was zero elsewhere. For every initial condition, the energy $E = 1$ and helicity $H = 1.55$ were the same, while the phases of velocity variables were random. Since the stiffness characterizing the original shell model equations is removed in the renormalized description, we were able to study a very large range of shell numbers ($N = 120$ total shells are used in most simulations) with a shell-to-shell ratio $\lambda = 2$. Each simulation was stopped as soon as the energy reached the highest wave number. Given the possibility to achieve extremely high wave numbers, care must be taken when measuring the helicity H or other helicity-sensitive quantities [in general, all observables of the form $k_n^\alpha(|u_n^+|^\beta - |u_n^-|^\beta)$], because huge cancellations might take place at high wave numbers and quadruple precision arithmetic is required for large N.

Two types of limiting behavior were observed at large τ, depending on the model. Models SM1 and SM3 exhibit an attractor in the form of a traveling wave, which moves toward larger shell numbers n keeping a constant shape $W^\pm(\xi)$ and speed s [see Eq. (17)]. Models SM2 and SM4, on the other hand, show chaotic behavior with a solution moving in the same direction of large n. Figure 1 shows two representative cases of regular (left) and chaotic (right) dynamics. Both the energy E_n and the norm $|w_n^+|^2 + |w_n^-|^2$ spectra at each shell are shown at equally separated moments in renormalized time τ, showing clearly the traveling wave nature of the solution. In the first case, the wave has a constant profile and we say that the instanton is regular, while in the second case the profile fluctuates chaotically and we call the instanton chaotic.

At each time, the dynamics is effectively confined to a finite number of shells in the front of the propagating pulse, while in the tail of the solution, i.e., at smaller shell numbers n, the dynamics is frozen due to much larger characteristic time scales [see Figs. 1(a) and 1(b)]. Thinking in terms of the original time t, the dynamics is localized in the instants immediately preceding the blowup time t_c.

Figure 2 shows the relative enstrophy growth Ω/Ω_0 with τ and the corresponding logarithmic derivative $A = \frac{1}{\omega} \frac{d\omega}{d\tau}$ [see Eq. (14)] for the different models. We clearly distinguish two different behaviors. The enstrophy growth is exponential on average for large τ. However, the growth rate A stabilizes near specific values for models SM1 and SM3, where the attractor in the renormalized system is a traveling wave. On the contrary, a chaotically pulsating A is observed for models SM2 and SM4, where the attractor is chaotic.

By approaching the infinite shell number $n \to \infty$ as $\tau \to \infty$ (corresponding to $t \to t_c^-$), the energy gets a specific distribution over the whole range of scales, as shown in Fig. 3. The regular instanton (models SM1 and SM3) leaves behind an asymptotically exact power-law energy spectrum,
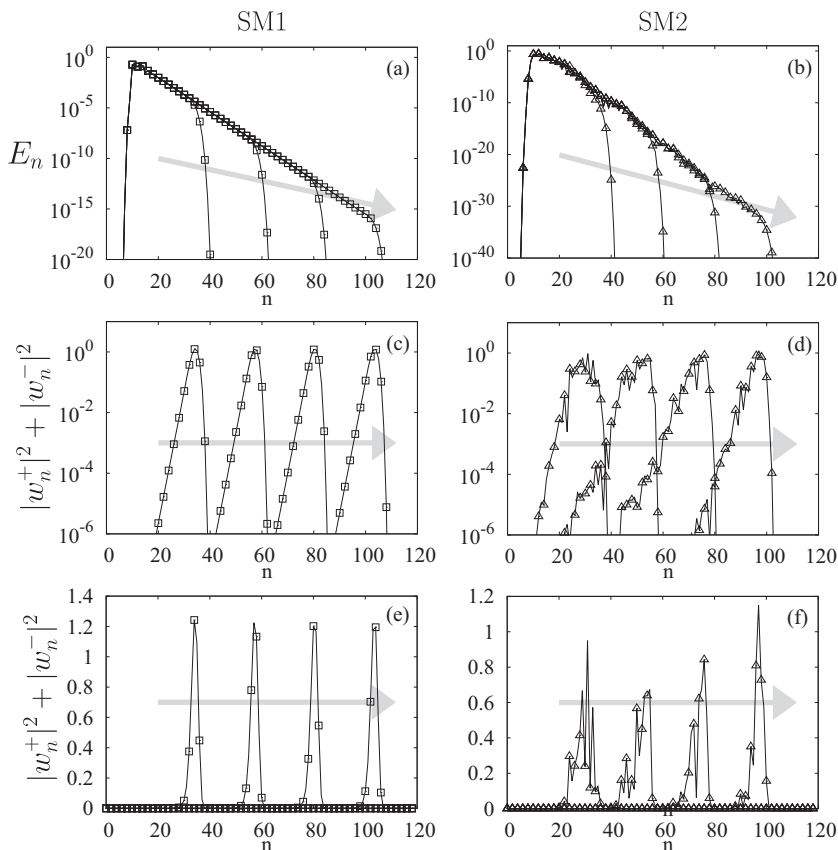
FIG. 1. Snapshots of the solution of Eqs. (12) and (13) at different, equally separated, moments in the renormalized time τ, for two models with a regular and a chaotic instanton: energy spectrum for (a) model SM1 and (b) model SM2 and norm spectrum $|w_n^+|^2 + |w_n^-|^2$ for (c) model SM1 and (d) model SM2. Panels (e) and (f) show the same curves as (c) and (d), without logarithmic scale on the y axis. The arrows in the background show the direction of increasing τ.

while the chaotic instanton (models SM2 and SM4) leads to the power-law energy spectrum only on average, and a fluctuating component remains at all scales. The scaling exponents of the energy spectra vary greatly from model to model, a hint that the different helical nonlinear interactions (models) may have a different degree of influence over the dynamics of the whole system when coupled together. Figure 3 presents results for a number of different simulations, which have the same initial amplitudes for the $u_n^\pm$ limited to $n \in [10,14]$ but with different phases, randomly chosen. An interesting feature that distinguishes the chaotic instantons of model SM2 from the one of model SM4 is the increasing spread of the energy profiles at small scales shown by the former. Simulations with larger total shells N indicate that this spread may be explained as the intermittency phenomenon, in the context of dynamical systems [35]: In the renormalized variables, the wave undergoes irregular jumps between periodic and chaotic dynamics and among regimes characterized by different scalings. This is shown in Fig. 4, where we plot the probability density function (PDF) of the local scaling exponents α of the energy spectrum $E_n \sim k_n^\alpha$ for the two models SM2 and SM4. The scaling exponents α are related to y in Eq. (19) by $\alpha = 2(y - 1)$. They are calculated by performing a power-law fit on several sections, 40 shells long, taken from the energy spectrum curves (Fig. 3) (limited to $20 \leqslant n \leqslant 100$). As one can see, while model SM4 has a distribution
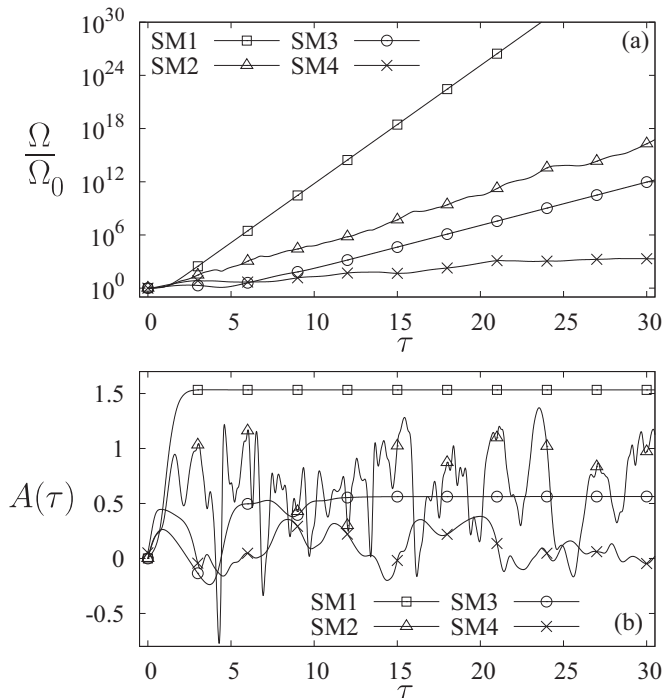
FIG. 2. (a) Relative enstrophy Ω/Ω_0 growth with renormalized time τ for different models in a single realization of the instanton. (b) Logarithmic derivative $A = \frac{1}{\omega}\frac{d\omega}{d\tau}$ for different models. The curves stabilize near specific values (regular instantons, SM1 and SM3) or oscillate chaotically (chaotic instantons, SM2 and SM4).

peaked around $\alpha = -1.6$, for model SM2 we have a wider spectrum of values with a strong peak around $\alpha = -0.85$ and a less pronounced peak around $\alpha = -1.3$.

V. HELICAL STRUCTURE

Let us now analyze the helical component of the instantonic solutions. Model SM1, being made of two decoupled Sabra models, will develop also decoupled instantons for each submodel with different blowup times that depend on the initial condition. As a result, only the fastest instanton will dominate the dynamics asymptotically and the connection among helicity and energy spectrum is trivial: $H_n = (-)^n k_n E_n$. The very same happens for model SM4, with the only difference that $H_n = k_n E_n$ (or $H_n = -k_n E_n$).

On the other hand, in models SM2 and SM3 all positive and negative helical modes are coupled and the dynamics is richer. In Fig. 5(a) we show the helicity spectrum for models SM2 and SM3 at a late time. We immediately notice that for model SM3 there is a fast recovery of parity invariance, $u_n^{\pm} \mapsto u_n^{\mp}$, as suggested by the alternation of positive (black) and negative (gray) signs in H_n. A further confirmation of this recovery comes from the power-law scaling

$$E_n = e_n k_n^{-\xi_E}, \quad H_n = h_n k_n^{-\xi_H}, \tag{22}$$

where e_n and h_n are $O(1)$ functions of n. Exploiting (22) in the helical decomposition (7), we can write

$$|u_n^+|^2 = \left(e_n k_n^{-\xi_E} + h_n k_n^{-\xi_H-1}\right)/2, \tag{23}$$

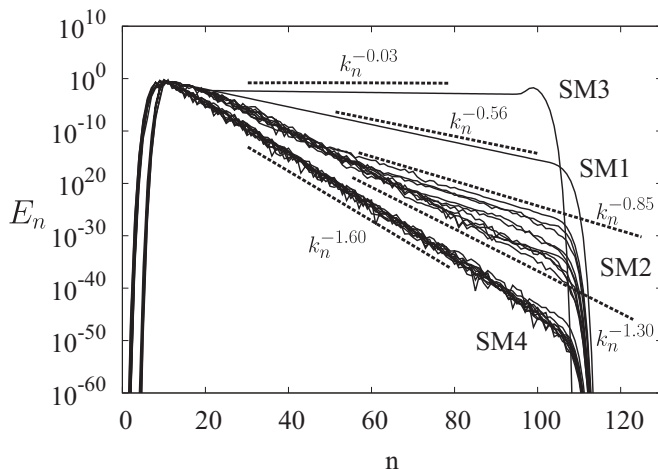$$|u_n^-|^2 = \left(e_n k_n^{-\xi_E} - h_n k_n^{-\xi_H-1}\right)/2, \tag{24}$$

FIG. 3. Late-time ($t \to t_c^-$) energy spectrum E_n of the instantons for different helical models. Multiple realizations are shown for the chaotic instantons (models SM2 and SM4). The dotted lines show scaling laws that best fit the different curves.

with a power law for the relative helicity

$$\frac{|u_n^+|^2 - |u_n^-|^2}{|u_n^+|^2 + |u_n^-|^2} \sim k_n^{\xi_E - \xi_H - 1}. \tag{25}$$

Looking at Figs. 3 and 5(a), we conclude that model SM3 with $\xi_E \approx \xi_H$ has a strong recovery of mirror symmetry for small scales with the power law $k_n^{\xi_E - \xi_H - 1} \approx k_n^{-1}$.

On the other hand, for model SM2 one has $\xi_E \approx \xi_H + 1$. Hence, the chaotic behavior does not produce an exact cancellation of the leading mirror-symmetric terms and we observe $k_n^{\xi_E - \xi_H - 1} \sim 1$ in (25). Nevertheless, the PDF of the helicity at different shell numbers indicates that even model SM2 eventually recovers parity invariance. As shown in Fig. 5(b), the PDF of H_n is strongly skewed at shell numbers where the (helical) initial condition is nonzero ($n = 12$), while the same PDF becomes more and more symmetric at increasing n. It is then argued that model SM2 will recover
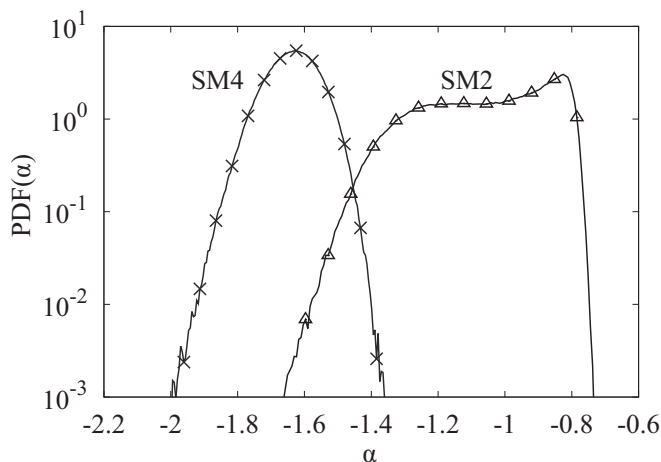

FIG. 4. PDF of local scaling exponents α of the energy spectrum E_n (see Fig. 3) for models SM2 and SM4.
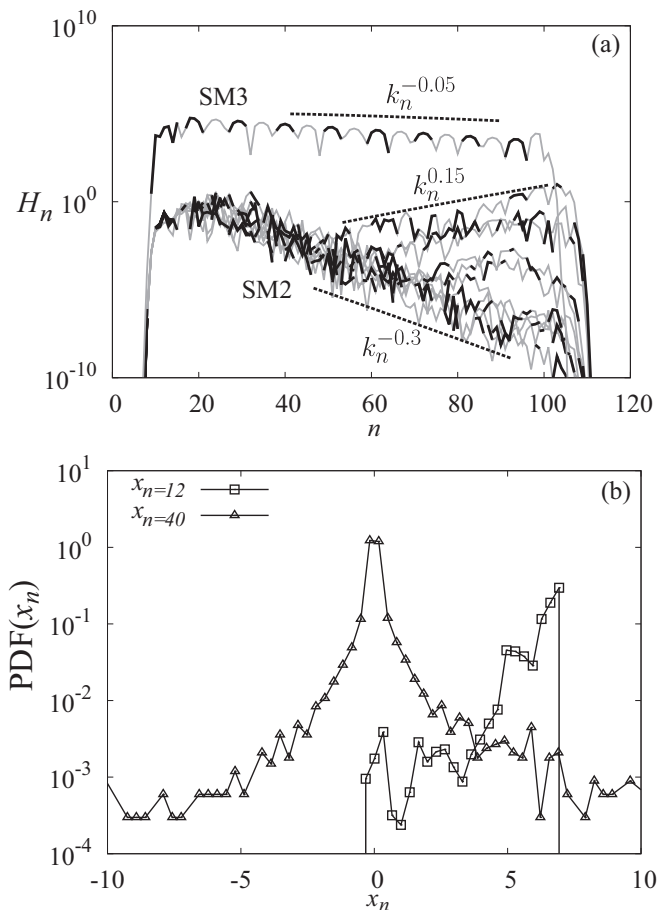
FIG. 5. (a) Late-time ($t \to t_c^-$) helicity spectra H_n of the instantons for different helical shell models. Multiple realizations are shown for the chaotic instantons (model SM2). The two different models are shifted vertically for clarity The segments in gray represent negative values. (b) Late-time PDF of $x_n \equiv \frac{H_n}{\sqrt{\langle H_n^2 \rangle - \langle H_n \rangle^2}}$ for model SM2 at different shell numbers n.

parity symmetry in a statistical sense when averaged over different instantonic solutions. However, given the huge fluctuations in the energy and helicity spectra, this test would require an extremely high number of instantons to converge.

VI. PROPERTIES OF INSTANTONS VS DEVELOPED TURBULENT DYNAMICS

In this section we study how the dynamics of the instantons compare with the stationary dynamics obtained in the same models with a forcing and viscous dissipation. In particular, we are interested in understanding whether a correlation exists between the direction of the stationary energy transfer and the transfer properties of instantonic solutions, together with issues connected to the anomalous scaling of the full stationary solutions.

In the stationary case, the energy transfer has been already studied in the literature [22,28,36], showing that models SM1–SM3 have mainly a forward energy cascade (from large to small scales) while model SM4 have a backward energy transfer but close to a quasiequilibrium state [36,37]. Recently, a model (SM2E) with the same helical structure as SM2 and second-neighbor interactions

TABLE II. Summary of the dynamical properties of helical shell model (4) and (5) and model (26) and (27) in both the blowup and stationary regimes. Here α is the scaling exponent of the energy spectrum for the instanton. We recall that in the stationary regime, a forward energy cascade induces a Kolmogorov spectrum $E_n \sim k_n^{-2/3}$.

| Model | Instanton dynamics | | | Stationary dynamics | |
	Type	Energy transfer	α	Intermittency	Energy dynamics
SM1	regular	forward	-0.56	yes	forward cascade
SM2	chaotic	forward	$-1.3 < \alpha < -0.85$	no	forward cascade
SM2E	chaotic	backward	$-1.6 < \alpha < -1.1$	no	backward cascade
SM3	regular	forward	-0.03	yes	forward cascade
SM4	chaotic	backward	$\simeq -1.6$	no	backward flux + quasiequilibrium

among modes k_n, k_{n+2}, k_{n+3} was introduced in order to get a well developed inverse energy cascade regime, motivated by theoretical arguments based on the structure of the triadic interactions [28]:

$$\dot{u}_n^+ = i(ak_{n+2}u_{n+3}^- u_{n+2}^{-*} + bk_n u_{n+1}^+ u_{n-2}^{-*} + ck_{n-1}u_{n-1}^+ u_{n-3}^-) + f_n^+ - \nu k_n^2 u_n^+, \tag{26}$$

$$\dot{u}_n^- = i(ak_{n+2}u_{n+3}^+ u_{n+2}^{+*} + bk_n u_{n+1}^- u_{n-2}^{+*} + ck_{n-1}u_{n-1}^- u_{n-3}^+) + f_n^- - \nu k_n^2 u_n^-, \tag{27}$$

where, for $\lambda = 2$, the model constants are $a = 1$, $b = -9/4$, and $c = -5/4$. Model SM2E also develops a chaotic instanton with a slope for the energy spectrum around $\alpha = -1.4$ (discussed later).

A. Stationary dynamics

A summary of the energy transfer direction for all five models considered here is given in Table II. In the same table we also summarize what is known about the scaling properties of the stationary dynamics for all models. Scaling is here intended in terms of the structure functions for the full forced and viscous dynamics, defined as

$$S_p(k_n) = \langle |u_n^+|^p + |u_n^-|^p \rangle \sim k_n^{-\zeta_p}, \tag{28}$$

where with $\langle \cdots \rangle$ we mean the average over the statistically stationary ensemble and by ζ_p we denote the scaling exponents. For the case of three-dimensional Navier-Stokes turbulence, it is empirically known that the equivalent of (28) written for velocity increments in real space, $\langle (\delta_r v)^p \rangle \sim r^{\zeta_p}$, develops anomalous corrections: The scaling exponents do not follow a linear dimensional law $\zeta_p - (p/3)\zeta_3 \neq 0$.

For the common choice $\lambda = 2$ the shell models SM1 and SM3 show anomalous exponents quantitatively very close to those of the full three-dimensional NSE. Other models do not show intermittent behavior: SM2 has a nonintermittent forward cascade and the structure functions scale with exponents very close to $\zeta_p = p/3$; SM4 has a forward helicity cascade, as for the case of the NSE restricted to evolve only on a given sign of helical modes [24], and the scaling exponents are very close to $\zeta_p = 2p/3$; finally SM2E has neither a forward energy cascade nor a forward helicity cascade, but the scaling exponents are still linear in p (model SM2E actually shows a forward cascade of a third positive-definite invariant; see [38] for details). In Fig. 6 we summarize the anomalous corrections for the stationary structure functions in the presence of viscous and forcing terms for all models.

From the above considerations we notice that there exists a correlation between the presence of chaotic instantons and the absence of small-scale statistically stationary anomalous scaling, at least for the evolution of each helical shell model separately. Furthermore, we note that the absence of anomalous scaling for the stationary statistics is also correlated to the existence of instantons with an
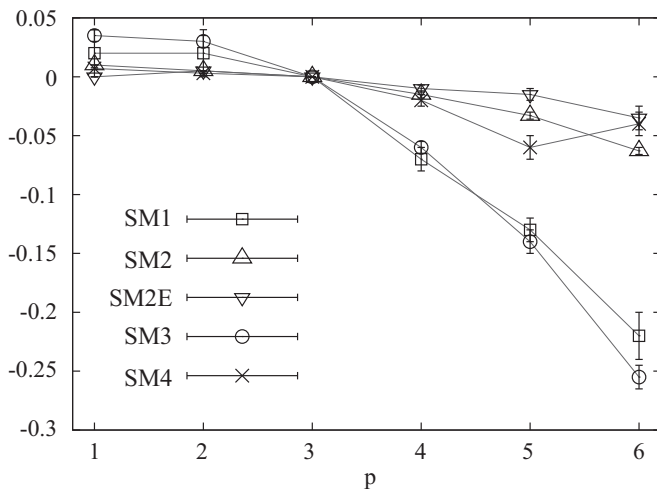
FIG. 6. Anomalous corrections $\Delta_p = \zeta_p - (p/3)\zeta_3$ to the scaling exponents of the structure functions $S_p(k_n)$ calculated in the forced-viscous regime, as functions of the order p, for the various helical shell models.

energy spectrum steeper than the dimensional Kolmogorov scaling $E_n \sim k_n^{-2/3}$. This follows from the condition $|\alpha| > 2/3$ in Table II.

The full Navier-Stokes dynamics corresponds to a mixture of the four helical classes, including models with all possible nonlocal interactions [28]. The behavior of the full coupled system may (or may not) inherit some properties of the individual models. In the shell model framework, this aspect can be studied by considering a linear combination of different models, e.g., by linearly coupling with a parameter $0 \leqslant z \leqslant 1$ the dynamical evolution of two models. In Fig. 7 we show the correlation between the anomalous correction to the sixth-order structure function $\Delta_6 = \zeta_6 - 2\zeta_3$ in
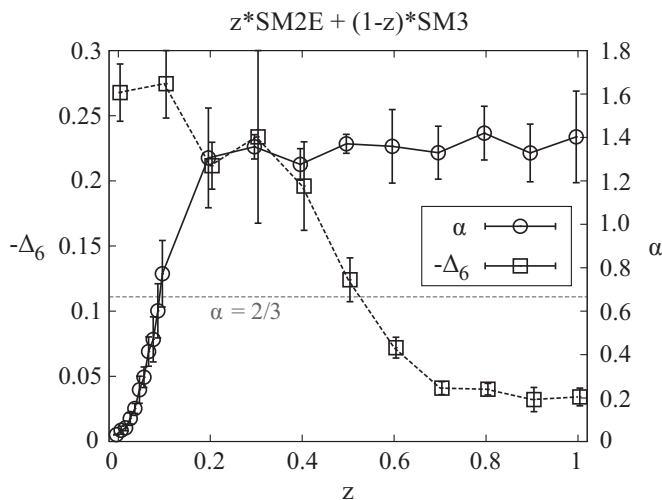

FIG. 7. Comparison between the instantonic solution and the forced-viscous system solution, for a linear combination of models SM2E and SM3, with coupling coefficients z and $1 - z$, respectively. The left axis is the anomalous correction to the sixth-order structure function $\Delta_6 = \zeta_6 - 2\zeta_3$ for the forced-viscous system solution. The right axis is the scaling exponent α of $|u_n^{\pm}| \sim k_n^{\alpha}$ for the instantonic solution. The gray line represents the Kolmogorov scaling $E_n \sim k_n^{-2/3}$.

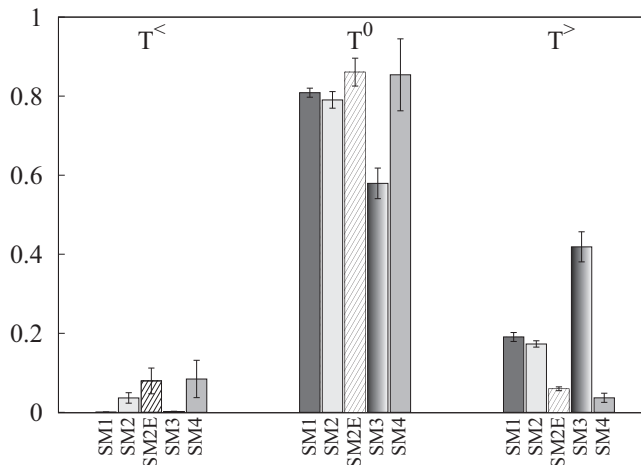FIG. 8. Energy transfers (29)–(31), from the scales where the initial condition is localized, towards larger $T^<$, smaller $T^>$, or the same scales T^0, for various models. The values are obtained by averaging over all the instantons in the ensemble and over different initial conditions (both differing in phases and in the number of shells where energy is initially present); the error bars show the standard deviation.

the forced-viscous system and the scaling exponent $\alpha = 2(y - 1)$ of E_n measured in the instantonic solution, for a linear combination of model SM3 (no inverse cascade and regular instanton with a slope less steep than Kolmogorov's) with model SM2E (inverse cascade and chaotic instanton with a slope steeper than Kolmogorov's). The transition from the very intense (regular, small $|\alpha|$) to the weak (chaotic, large $|\alpha|$) instanton and the transition from an intermittent to a nonintermittent dynamics in the forced-viscous regime occur at roughly the same value of z. The transition on the instanton slope is sharper. Moreover, the instanton becomes chaotic already for $z < 0.1$, weakening the statement about the existence of a strict correlation among the presence of anomalous scaling and the inviscid structure of the instantonic solutions observed for the pure models ($z = 0$ or $z = 1$). Figure 7 also shows that the transition to an intermittent scaling ($-\Delta_6 > 0$) is observed for values of α around the Kolmogorov scaling ($-2/3$). Notice that there exists a residual intermittency even in the region where the instanton has a slope $|\alpha| > 2/3$ ($z \gtrsim 0.6$). We cannot state if this effect is vanishing with increasing Reynolds number because of numerical limitations.

B. Energy transfer by instantons

In order to understand the transfer properties of instantonic solutions for each of the five models, we divided the shells inside the system into three domains: the interval of shells n where the instanton is initialized $I_0 = \{n_1 \leqslant n \leqslant n_2\}$ and the interval of shells at larger and smaller scales, respectively, $I^< = \{n < n_1\}$ and $I^> = \{n > n_2\}$. For each instanton, we measured the energy contained in each of the three ranges at a late time $t^* \approx t_c$ (very large τ). Normalizing this number by the total energy gives the fraction of energy transferred to larger and smaller scales, or kept in place, by a single instanton. Formally,

$$T_E^<(t^*) = \frac{1}{E} \sum_{n \in I^<} E_n(t^*), \tag{29}$$

$$T_E^0(t^*) = \frac{1}{E} \sum_{n \in I^0} E_n(t^*), \tag{30}$$

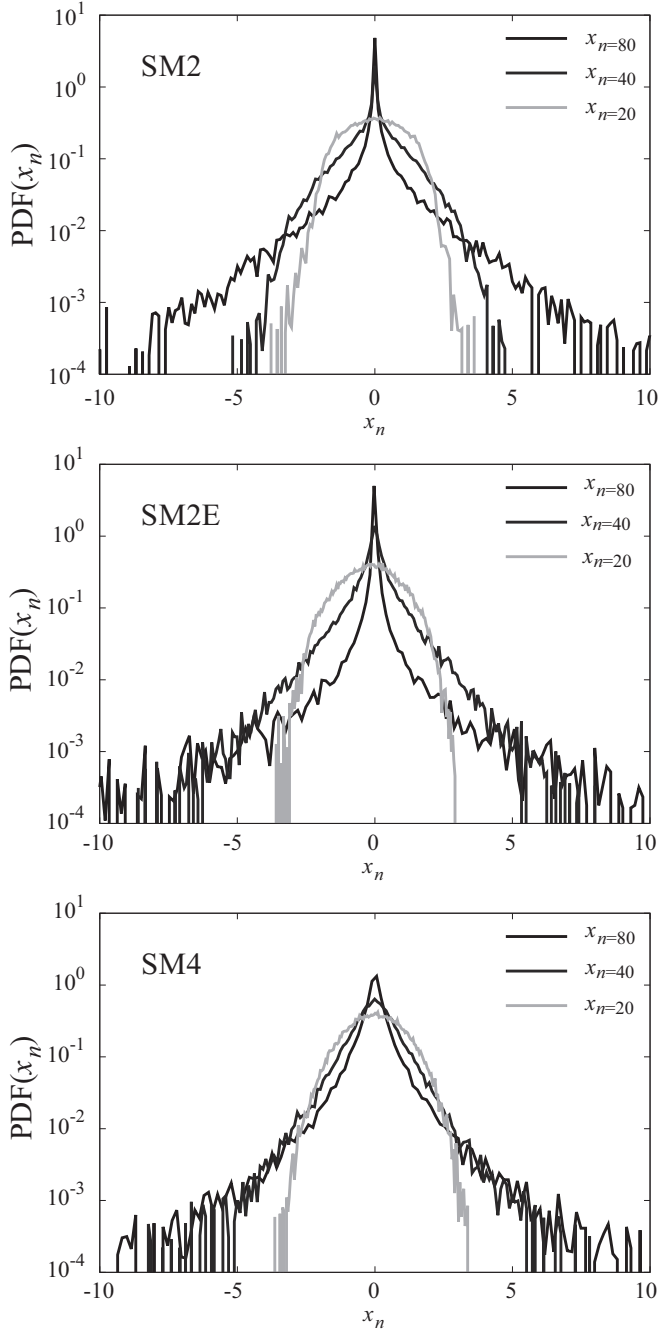$$T_E^>(t^*) = \frac{1}{E} \sum_{n \in I^>} E_n(t^*). \tag{31}$$

FIG. 9. PDF of $x_n \equiv \frac{\mathrm{Re}[u_n]}{\sqrt{\langle \mathrm{Re}[u_n]^2 \rangle}}$ (Re is the real part), at different scales identified by the shell number n, for models SM2, SM2E, and SM4.

The transfers $T_E^<$, T_E^0, and $T_E^>$ for all the models are shown in Fig. 8. These transfers are averaged over all the instantons in the ensemble and over different choices for the width of the interval I^0 (ranging from three to seven shells). We see that in general instantons do not transfer forward (to

small scales) a large amount of energy, in agreement also with what is shown in Fig. 3, except for instantons of SM3, which are able to downscale almost 40% of the initial energy. For the backward energy transfer, the main effect is detected for models SM2E and SM4. Despite the fact that the total amounts of transferred energy are not too big, it is remarkable that the energy transfer by instantons follows the same direction as the energy cascade in stationary turbulent dynamics (see Table II). In particular, model SM3 has a very clear predominance in transferring forward. This might be considered a good indication that instantons play a relevant role in such helical interactions. For the inverse cascade, the properties of models SM2E and SM4 are less compelling but are still present.

C. Intermittency of instantons

The presence of chaotic instantons for models SM2, SM2E, and SM4 might eventually lead to nontrivial anomalous scaling by themselves, without considering the whole forced and viscous dynamics. In Fig. 9 we show the PDF of the real part of u_n^+ for different values of the shell number n, where the statistics is obtained over $O(10^6)$ instantons. As one can see, model SM2 and SM2E show a imperfect rescaling of the standardized PDF, even though the statistics does not allow one to make a firm statement about a strong breaking of self-similarity. The possibility that by allowing the instantons to travel for a much larger number of shells they all converge on one single averaged scaling exponent cannot be ruled out. This would indicate the existence of a chaotic attractor in the renormalized dynamics.

VII. CONCLUSION

We have studied the finite-time blowup solutions (instantons) for a set of four families of helical shell models that follow the exact decomposition of the Navier-Stokes equations in helical states. Four models SM1–SM4 were studied with the simplest short-range interactions allowed by the symmetries of the equations; an extra model SM2E was also considered with more nonlocal interactions in order to study also systems with an inverse energy cascade. When the models are initialized with energy at the large scales, the blowup solutions generate coherent structures that travel toward small scales. For models SM1 and SM3, the instantons are regular, less steep than the Kolmogorov scaling, and develop a self-similar asymptotic profile. For model SM4, the self-similarity holds only on average, with the instanton showing a chaotic evolution around a well defined mean profile. For models SM2 and SM2E, the instantons are again chaotic and oscillating among different states, apparently breaking a self-similar propagation, even on average. All models SM2, SM2E, and SM4 have instantons with spectral slopes steeper than Kolmogorov.

The regularity or chaoticity of the blowup solutions correlates with the distinction of the various helical interactions based on the linear stability analysis of a single triad [23]. In fact, the models with regular instantons (SM1 and SM3) belong to categories of helical interactions where the smallest wave number in a triad transfers energy to the other two, while the models with chaotic instantons (SM2, SM2E, and SM4) belong to categories in which the middle wave number in a triad transfers energy to the other two.

Another interesting correlation was observed concerning the intermittency in the stationary dynamics for the same helical shell models. In fact, the stationary regimes of both models SM1 and SM3 show anomalous scaling exponents for the velocity structure functions, quantitatively very similar to those of the Navier-Stokes turbulence [7,8,22]. On the contrary, models SM2, SM2E, and SM4 do not show significant anomalous correction [28,36]. Combining two models, e.g., SM2E and SM3, one observes that whenever the small-scale stationary statistics is significantly intermittent, the instanton is less steep than the dimensional Kolmogorov scaling, independently of whether or not it is chaotic. This observation supports the idea that intermittency in the forced-viscous dynamics is influenced by instantons, if they are intense enough.

We also found a correlation between the energy transfers observed in the instantons and the energy fluxes measured in the stationary dynamics. All the models characterized by constant fluxes

of energy toward small scales have instantons in which the dominant energy transfer is toward small scales and vice versa.

Finally, we have shown that model SM3 has a faster recovery of parity invariance at small scales compared to the other models. This seems to be the case also in the stationary dynamics [31]. Furthermore, model SM3 is known to have a dynamics that is very robust with respect to variations in the model parameters such as the shell-to-shell ratio λ or the dimensionality of the second inviscid invariant [22]. All these clues reinforce the idea that the helical interaction present in model SM3 is actually the dominant component of the 3D Navier-Stokes dynamics.

ACKNOWLEDGMENTS

---

[1] U. Frisch, *Turbulence: The Legacy of A. N. Kolmogorov* (Cambridge University Press, Cambridge, 1995).

[2] A. Obukhov, Some general characteristic equations of the dynamics of the atmosphere, Izv. Akad. Nauk SSSR, Fiz. Atmos. Okeana **7**, 695 (1971).

[3] E. B. Gledzer, System of hydrodynamic type admitting two quadratic integrals of motion, Sov. Phys. Dokl. **18**, 216 (1973).

[4] V. N. Desnianskii and E. A. Novikov, Evolution of turbulence spectra toward a similarity regime, Izv. Akad. Nauk SSSR, Fiz. Atmos. Okeana **10**, 127 (1974).

[5] M. Yamada and K. Ohkitani, The inertial subrange and non-positive Lyapunov exponents in fully-developed turbulence, Prog. Theor. Phys. **79**, 1265 (1988).

[6] M. H. Jensen, G. Paladin, and A. Vulpiani, Intermittency in a cascade model for three-dimensional turbulence, Phys. Rev. A **43**, 798 (1991).

[7] V. S. L'vov, E. Podivilov, A. Pomyalov, I. Procaccia, and D. Vandembroucq, Improved shell model of turbulence, Phys. Rev. E **58**, 1811 (1998).

[8] L. Biferale, Shell models of energy cascade in turbulence, Annu. Rev. Fluid Mech. **35**, 441 (2003).

[9] T. Bohr, M. H. Jensen, G. Paladin, and A. Vulpiani, *Dynamical Systems Approach to Turbulence* (Cambridge University Press, Cambridge, 2005).

[10] P. D. Ditlevsen, *Turbulence and Shell Models* (Cambridge University Press, Cambridge, 2010).

[11] D. Pisarenko, L. Biferale, D. Courvoisier, U. Frisch, and M. Vergassola, Further results on multifractality in shell models, Phys. Fluids A **5**, 2533 (1993).

[12] A. A. Mailybaev, Blowup as a driving mechanism of turbulence in shell models, Phys. Rev. E **87**, 053011 (2013).

[13] T. Dombre and J. L. Gilson, Intermittency, chaos and singular fluctuations in the mixed Obukhov-Novikov shell model of turbulence, Physica D **111**, 265 (1998).

[14] I. Daumont, T. Dombre, and J. L. Gilson, Instanton calculus in shell models of turbulence, Phys. Rev. E **62**, 3592 (2000).

[15] G. Falkovich, I. Kolokolov, V. Lebedev, and A. Migdal, Instantons and intermittency, Phys. Rev. E **54**, 4896 (1996).

[16] V. Gurarie and A. Migdal, Instantons in the Burgers equation, Phys. Rev. E **54**, 4908 (1996).

[17] E. Balkovsky, G. Falkovich, I. Kolokolov, and V. Lebedev, Intermittency of Burgers' turbulence, Phys. Rev. Lett. **78**, 1452 (1997).

[18] L. Biferale, I. Daumont, T. Dombre, and A. Lanotte, Coherent structures in random shell models for passive scalar advection, Phys. Rev. E **60**, R6299 (1999).

[19] A. I. Chernykh and M. G. Stepanov, Large negative velocity gradients in Burgers turbulence, Phys. Rev. E **64**, 026306 (2001).

[20] V. S. L'vov, Quasisolitons and asymptotic multiscaling in shell models of turbulence, Phys. Rev. E **65**, 026309 (2002).

[21] T. Grafke, R. Grauer, and T. Schäfer, The instanton method and its numerical implementation in fluid mechanics, J. Phys. A **48**, 333001 (2015).

[22] R. Benzi, L. Biferale, R. M. Kerr, and E. Trovatore, Helical shell models for three-dimensional turbulence, Phys. Rev. E **53**, 3541 (1996).

[23] F. Waleffe, The nature of triad interactions in homogeneous turbulence, Phys. Fluids A **4**, 350 (1992).

[24] L. Biferale, S. Musacchio, and F. Toschi, Inverse Energy Cascade in Three-Dimensional Isotropic Turbulence, Phys. Rev. Lett. **108**, 164501 (2012).

[25] L. Biferale, S. Musacchio, and F. Toschi, Split energy-helicity cascades in three-dimensional homogeneous and isotropic turbulence, J. Fluid Mech. **730**, 309 (2013).

[26] G. Sahoo and L. Biferale, Disentangling the triadic interactions in Navier-Stokes equations, Eur. Phys. J. E **38**, 1 (2015).

[27] A. Alexakis, Helically decomposed turbulence, J. Fluid Mech. **812**, 752 (2017).

[28] M. De Pietro, L. Biferale, and A. A. Mailybaev, Inverse energy cascade in nonlocal helical shell models of turbulence, Phys. Rev. E **92**, 043021 (2015).

[29] A. A. Mailybaev, Renormalization and universality of blowup in hydrodynamic flows, Phys. Rev. E **85**, 066317 (2012).

[30] V. A. Belinskii, I. M. Khalatnikov, and E. M. Lifshitz, Oscillatory approach to a singular point in the relativistic cosmology, Adv. Phys. **19**, 525 (1970).

[31] N. M. Rathmann and P. D. Ditlevsen, Role of helicity in triad interactions in three-dimensional turbulence investigated by a new shell model, Phys. Rev. E **94**, 033115 (2016).

[32] P. Constantin, B. Levant, and E. S. Titi, Regularity of inviscid shell models of turbulence, Phys. Rev. E **75**, 016304 (2007).

[33] A. Cheskidov, Blow-up in finite time for the dyadic model of the Navier-Stokes equations, Trans. Am. Math. Soc. **360**, 5101 (2008).

[34] A. A. Mailybaev, Bifurcations of blowup in inviscid shell models of convective turbulence, Nonlinearity **26**, 1105 (2013).

[35] E. Ott, *Chaos in Dynamical Systems* (Cambridge University Press, Cambridge, 2002).

[36] P. D. Ditlevsen and I. A. Mogensen, Cascades and statistical equilibrium in shell models of turbulence, Phys. Rev. E **53**, 4785 (1996).

[37] T. Gilbert, V. S. L'vov, A. Pomyalov, and I. Procaccia, Inverse Cascade Regime in Shell Models of Two-Dimensional Turbulence, Phys. Rev. Lett. **89**, 074501 (2002).

[38] N. M. Rathmann and P. D. Ditlevsen, Pseudo-invariants causing inverse energy cascades in three-dimensional turbulence, arXiv:1610.03879.